ELSEVIER

S0032-3861(96)00237-6

Polymer Vol. 37 No. 23, pp. 5123–5129, 1996

0032-3861/96/$15.00+0.00

Fracture of binary blends of linear and branched polyethylene

M. Hedenqvist, M. T. Conde Braña and U. W. Gedde*
Department of Polymer Technology, Royal Institute of Technology, S-100 44 Stockholm, Sweden

and J. Martinez-Salazar
Instituto de Estructura de la Materia, CSIC, Serrano 119, 28006 Madrid, Spain
(Received 16 December 1994; revised 25 July 1995)

The fracture behaviour of binary mixtures of low molar mass linear polyethylene (L2.5: $\bar{M}_w = 2500\,g\,mol^{-1}$, $\bar{M}_w/M_n = 1.15$) and higher molar mass linear and branched polyethylenes has been studied. The average tie-chain concentration of the different samples has been indirectly estimated. It was found that the true stress at fracture, fracture strain and fracture energy increased with the calculated average tie-chain concentration for all the binary blends. For the binary mixtures of L2.5 and the higher molar mass linear polyethylenes, there is no unique relationship between true stress at fracture and calculated average tie-chain concentration, suggesting that segregation of L2.5 is an important factor determining the strength of these samples. The fact that the L2.5/branched polyethylene blends with intimately mixed constituents exhibited a higher strength than the L2.5/linear polyethylene mixtures, with a distinct segregation of L2.5, could be explained as being due to the higher average tie-chain concentration in the former blends. Copyright © 1996 Elsevier Science Ltd.

(Keywords: binary blends; linear polyethylene; branched polyethylene; fracture; morphology)

INTRODUCTION

The crystallization kinetics of binary mixtures of low molar mass linear polyethylene (PE) and higher molar mass linear and branched PE have been reported in a series of papers[1–6]. Blends of a low molar mass linear PE sharp fraction ($\bar{M}_w = 2500\,g\,mol^{-1}$) and higher molar mass linear PE fractions ($\bar{M}_w > 66\,000\,g\,mol^{-1}$) crystallized separately under most conditions[2]. The high molar mass component crystallized first in dominant crystal lamellae and the low molar mass component crystallized later in subsidiary crystal lamellae[2]. Transmission electron microscopy of binary mixtures of L2.5 and branched PE of higher molar mass, similar to one of the polymers studied here, showed predominant co-crystallization[6]. Partial segregation of L2.5 was revealed only in the case of blends of the highest content of L2.5 (80%)[6].

It is known from earlier work on PE with a broad molar mass distribution that fracture propagates preferentially through domains of segregated low molar mass material[7]. It was suggested that the low concentration of tie-chains in the low molar mass material was the reason for its low strength[7]. The present paper can be regarded as a continuation of this work. The fracture behaviour of mixtures exhibiting pronounced molar mass segregation typical of blends of linear PE samples of different molar mass is compared with that of samples consisting of more intimately mixed low molar mass linear and higher molar mass branched PE.

* To whom correspondence should be addressed

EXPERIMENTAL

Binary mixtures of different compositions consisting of a linear PE sharp fraction ($\bar{M}_w = 2500\,g\,mol^{-1}$, $\bar{M}_w/\bar{M}_n = 1.15$), referred to as L2.5, purchased from Polymer Laboratories Ltd, UK, and higher molar mass linear and branched PE grades were prepared by solution mixing[4]. The higher molar mass samples were experimental grades produced by Neste Polyeten AB, Sweden, and are referred to as BE1.5 ($\bar{M}_w = 127\,000\,g\,mol^{-1}$; $\bar{M}_w/M_n = 7.5$; 1.5 mol% ethyl branches), L144 ($\bar{M}_w = 144\,000\,g\,mol^{-1}$; $\bar{M}_w/\bar{M}_n = 10.3$; linear polymer) and L95 ($\bar{M}_w = 95\,000\,g\,mol^{-1}$; $\bar{M}_w/\bar{M}_n = 7.2$; linear polymer). Data for the average molar mass and degree of chain branching were obtained by size exclusion chromatography and C-13 nuclear magnetic resonance spectroscopy[4]. Samples with the dimensions of 50 mm (length), 18 mm (width), and 3–4 mm (thickness) were made by compression moulding at 445 K followed by cooling at 2 or 30 K min^{-1}. The samples were single-edged-notched along their width to a depth of 0.5 ± 0.1 mm with fresh razor blades with a radius of 3 μm at the tip.

The specimens were drawn at 294 ± 1 K and 40% relative humidity with a strain rate of 10 mm min^{-1} in an Instron Universal Testing Instrument Model 1122 calibrated according to standard procedures. The distance between the clamps was 30 mm. At least five specimens of each material were tested. The load–time deflection curves were recorded until fracture occurred. Fractography was performed on gold-sputtered samples in an ISI Super Mini SEM to determine the thickness of the

razor blade notch and the sizes of the slow and rapid crack growth zones.

A pinhole-collimated Rigaku camera attached to a Cu rotating anode source operating at 140 mA and 40 kV was used to obtain the small angle X-ray scattering (SAXS) patterns. The sample-to-film distance was 440 mm. The exposure times were approximately 48 h. The scattered intensities were obtained by using a Perkin–Elmer two-dimensional microdensitometer with a 'pixel' size of 50 μm within a square area of $15 \times 15\,mm^2$. The scattered intensity (I) was obtained as a function of scattering angle (θ) by averaging a number of diametrical readings through the centre of the main beam position, the background being subtracted from the intensity curve. The reduced scattered intensity curve [$I = f(\theta)$] was divided into a Gaussian and a Lorentzian component according to equation (1) using a least-squares-fitting procedure[8]:

$$I = I_0 e^{-\left(\frac{2(\theta-\theta_0)}{a_0}\right)^2} + \frac{I_1}{\left[1+\left(\frac{2}{a_1}(\theta-\theta_1)\right)^2\right]^2} \quad (1)$$

where I_0 and I_1 are scattered intensities associated with the Gaussian and the Lorentzian functions respectively, and θ_0, θ_1, a_0 and a_1 are adjustable variables. The Lorentz correction[9] was applied: the s value (s_{max}) associated with the maximum in the expression $I(\text{Lorentz}) \cdot s^2 = f(s)$ [$s = 2\sin\theta/\lambda$, λ = wavelength] was determined and the long period (L, see *Figure 1*) was obtained according to:

$$L = \frac{1}{s_{max}} \quad (2)$$

The melting endotherms of the samples were obtained in a Perkin–Elmer DSC-7 at a heating rate of 10 K min^{-1} and the recorded values of heat of fusion (Δh_f) were transformed into mass crystallinity (w_c) using the total enthalpy method[10], using 293 kJ kg^{-1} as the heat fusion (Δh_f^0) for 100% crystalline polymer at the equilibrium melting point, T_m^0 (418.5 K)[11]:

$$w_c = \frac{\Delta h_f}{\Delta h_f^0 - \int_{T_1}^{418.5} (c_{pa} - c_{pc})\,dT} \quad (3)$$

where T_1 is an arbitrary temperature below the melting range, and c_{pa} and c_{pc} are the specific heats of the amorphous and crystalline components, respectively. Data for c_{pa} and c_{pc} presented by Wunderlich and Baur[12] have been used. The Thomson–Gibbs equation[13] was used to calculate the crystal thickness (*Figure 1*):

$$L_{c,DSC} = \frac{2\sigma T_m^0}{(T_m^0 - T_m)\Delta h_f^0 \rho_c} \quad (4)$$

where $L_{c,DSC}$ is the crystal thickness, σ is the fold surface free energy (93 mJ m^{-2}) and ρ_c is the crystal phase density (1000 kg m^{-3})[14]. The long period is given by:

$$L = \frac{L_{c,DSC}\left[w_c + \left(\frac{\rho_c}{\rho_a}\right)(1-w_c)\right]}{w_c} \quad (5)$$

where ρ_a is the density of the amorphous component (855 kg m^{-3})[14].

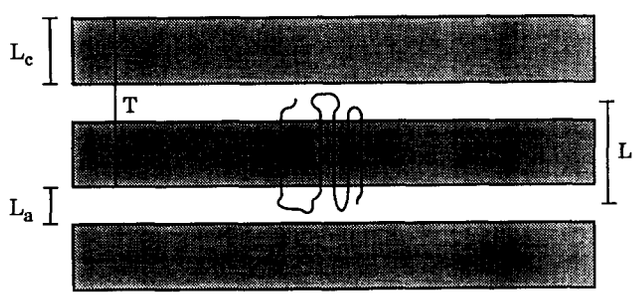

Figure 1 Lamellar structure of polyethylene containing a tie-chain (T), long period (L), crystal thickness (L_c) and amorphous thickness (L_a)

RESULTS AND DISCUSSION

The fracture data are summarized in *Tables 1* and *2*. Ductile fracture with necking was observed in L2.5/BE1.5 (0/1 and 0.2/0.8) of both cooling rates and in L2.5/L144 (0/1) cooled at 30 K min^{-1}. The other samples exhibited apparently brittle fractures although SEM fractography revealed a great many fibrils in the fracture surfaces (*Table 2*). It was possible to distinguish the slow crack growth zone in the surface fractures. When it was present, the slow crack growth zone was always located adjacent to the notch and its propagation length usually varied along the width of the specimens (*Figure 2*). The slow crack growth zone always contained thicker and wider fibrils at a significantly higher concentration than the rapid crack growth zone (*Table 2*, *Figure 2*). The size of the slow crack growth zone relative to the cross-sectional area of the specimen increased both with decreasing content of L2.5 and with increasing cooling rate (*Table 2*). The relative size of the slow crack growth zone was also significantly greater for blends of L2.5/BE1.5 than for blends of L2.5/L144 with the same L2.5 content (*Table 2*). Samples with the highest L2.5 content showed no slow crack growth zone, and a lack of fibrils in the fracture surface in these samples was also apparent. This behaviour was observed in blends of L2.5/L144 with a L2.5 content equal to or greater than 60% and in L2.5/BE1.5 with a L2.5 content of 80%.

The data for true stress at fracture presented in *Table 1* refer to the area of the rapid crack growth zone. Ductile fracture sometimes occurred in steps leading to an estimated 20% uncertainty in the true stress values for these specimens. The higher ductility of the L2.5/BE1.5 blends compared to the blends of L2.5/L144 and L2.5/L95 is demonstrated in the data of *Table 1*. Ductile fracture occurred in the L2.5/BE1.5 blends at higher L2.5 contents than in blends of L2.5/L144 and of L2.5/L95. The true stress values were also generally higher for the L2.5/BE1.5 blends than for L2.5/L144 (*Figure 3*). The difference between the two series of blends was significant for the blends of low L2.5 content and decreased with increasing content of L2.5, finally approaching the same value in samples with a high content of L2.5. The second series of linear PE blends, L2.5/L95, exhibited even lower true stress values than the L2.5/L144 blends (*Table 1*). The fracture data of L2.5/L144 and L2.5/L95 exhibited a cooling-rate dependence, whereas the blends of L2.5/BE1.5 showed no such dependence. *Table 1* shows that the fracture energy, i.e. the integrated initial

Table 1 Fracture data for blends investigated in this study

Sample		Fracture type[a]	σ_{nom}[b] (MPa)	σ_{true}[c] (MPa)	ε[d]	Fracture energy (J)[e]
L2.5/L144						
2 K min^{-1}	0 L2.5	b	24.1 ± 3.1	133.5 ± 45.8	0.127 ± 0.032	4.6 ± 1.8
	0.2 L2.5	b	17.0 ± 1.7	23.2 ± 3.1	0.046 ± 0.007	1.05 ± 0.27
	0.4 L2.5	b	13.1 ± 0.5	14.8 ± 0.8	0.027 ± 0.003	0.46 ± 0.08
	0.6 L2.5	b	7.9 ± 1.1	7.9 ± 1.1	0.049 ± 0.018	0.52 ± 0.18
	0.8 L2.5	b	4.4 ± 1.5	4.4 ± 0.5	0.026 ± 0.028	0.21 ± 0.26
30 K min^{-1}	0 L2.5	d	29.1 ± 0.8	139.2 ± 45.1	0.48 ± 0.14	11.2 ± 3.8
	0.2 L2.5	b	21.2 ± 1.4	28.2 ± 0.8	0.096 ± 0.018	2.8 ± 0.74
	0.4 L2.5	b	14.6 ± 0.8	17.2 ± 1.1	0.043 ± 0.003	0.81 ± 0.12
	0.6 L2.5	b	8.7 ± 0.4	8.7 ± 0.4	0.041 ± 0.010	0.49 ± 0.13
	0.8 L2.5	b	6.5 ± 1.2	6.5 ± 1.2	0.031 ± 0.016	0.29 ± 0.19
L2.5/L95						
2 K min^{-1}	0 L2.5	b	21.5 ± 1.1	49.6 ± 24.6	0.023 ± 0.004	0.40 ± 0.10
	0.2 L2.5	b	15.7 ± 2.3	22.8 ± 1.8	0.012 ± 0.002	0.12 ± 0.03
	0.4 L2.5	b	10.7 ± 1.3	12.9 ± 1.7	0.018 ± 0.005	0.24 ± 0.08
	0.6 L2.5	b	7.2 ± 1.8	7.2 ± 1.8	0.009 ± 0.006	0.09 ± 0.08
30 K min^{-1}	0 L2.5	b	21.5 ± 1.8	64.7 ± 49.9	0.063 ± 0.014	1.45 ± 0.39
	0.2 L2.5	b	15.3 ± 1.9	22.3 ± 1.4	0.016 ± 0.004	0.24 ± 0.07
	0.4 L2.5	b	9.4 ± 1.0	9.6 ± 1.4	0.020 ± 0.004	0.17 ± 0.04
	0.6 L2.5	b	7.6 ± 2.0	7.6 ± 2.0	0.011 ± 0.005	0.11 ± 0.07
	0.8 L2.5	b	3.6 ± 1.2	3.6 ± 1.2	0.005 ± 0.003	0.02 ± 0.01
L2.5/BE1.5						
2 K min^{-1}	0 L2.5	d	13.2 ± 0.8	81.6 ± 20.2	0.56 ± 0.12	2.9 ± 0.57
	0.2 L2.5	d	18.1 ± 1.2	53.3 ± 6.3	0.38 ± 0.14	1.5 ± 0.39
	0.4 L2.5	b	14.3 ± 0.6	34.1 ± 8.7	0.027 ± 0.008	0.39 ± 0.12
	0.6 L2.5	b	9.2 ± 0.6	10.9 ± 1.9	0.024 ± 0.004	0.23 ± 0.03
	0.8 L2.5	b	5.4 ± 2.9	5.4 ± 2.9	0.030 ± 0.020	0.14 ± 0.14
30 K min^{-1}	0 L2.5	d	11.3 ± 0.6	87.8 ± 13.3	0.73 ± 0.13	4.2 ± 0.38
	0.2 L2.5	d	16.5 ± 0.6	55.1 ± 10.7	0.49 ± 0.07	3.7 ± 0.75
	0.4 L2.5	b	12.2 ± 0.6	62.9 ± 27.0	0.030 ± 0.005	0.40 ± 0.10
	0.6 L2.5	b	9.7 ± 1.5	13.1 ± 1.0	0.017 ± 0.005	0.26 ± 0.12
	0.8 L2.5	b	5.5 ± 0.7	5.5 ± 0.7	0.005 ± 0.002	0.05 ± 0.02

[a] Fracture types b and d refer to brittle and ductile fracture respectively
[b] Nominal stress at fracture, i.e. fracture load divided by original cross-sectional area. Data are given as the average value ± standard deviation
[c] True stress at fracture, i.e. fracture load divided by actual cross-sectional area at fracture; data are given as the average value ± standard deviation
[d] Fracture strain referring to the total sample length; data are given as the average value ± standard deviation
[e] Fracture energy calculated by integration of the stress–strain curve; data are given as average value ± standard deviation

part of the stress–strain curve (before maximum load), generally exhibited the same kind of dependence on composition as the true stress data with the L2.5/L95 blends exhibiting the lowest values over the entire composition range.

It may be suggested that the strength of a given sample is closely related to its concentration of tie-chains[15]. The main problem is the present lack of methods for the assessment of tie-chain concentration. Another complicating factor is that the tie-chain concentration may vary considerably within the sample, particularly in samples with a pronounced molar mass segregation[7]. Brown *et al.*[16] have used an indirect method to determine the average tie-chain concentration. This method relies on the finding that the global dimension of a macromolecule, i.e. the average end-to-end distance (r), does not change on crystallization from the melt[17]. If the value of r of a given molecule expands over a distance greater than two crystal thicknesses (L_c) and one amorphous thickness (L_a) it is assumed to form a tie-chain (*Figure 1*). The average tie-chain concentration (P_{tc}) is thus given as:

$$P_{tc} = \frac{1}{3} \frac{\int_{\bar{L}_a + 2\bar{L}_c}^{\infty} r^2 e^{-\frac{3r^2}{2\langle r^2 \rangle_0}} dr}{\int_0^{\infty} r^2 e^{-\frac{3r^2}{2\langle r^2 \rangle_0}} dr} \quad (6)$$

where $\langle r^2 \rangle_0$ is the square of the end-to-end distance referring to molecules in the theta state, which for PE is approximately equal to $6.85nl^2$ (ref. 18); n being the number of carbon–carbon bonds and l being the carbon–carbon bond length. The crystal and amorphous average interlayer thicknesses ($\bar{L}_c$ and $\bar{L}_a$) were calculated from mass crystallinity and SAXS long periods (*Table 3*). The $2\bar{L}_c + \bar{L}_a$ data for the more slowly cooled samples were taken to be the same as for the more rapidly cooled samples. Using data for L144 led to an

Table 2 Fractographic characterization

Sample		Fracture type[a]	A_{scg} (%)[b]	SCG[c] Length/width/thickness (μm)	RCG[d] Length/width/thickness (μm)
L2.5/L144					
2 K min^{-1}	0 L2.5	brittle	77.6	6–140/12/1–2	100/0.5/0.5
	0.2 L2.5	brittle	26.0	2–11/1–10/< 1	90/0.5/0.5
	0.4 L2.5	brittle	10.8	< 1/< 1/< 1	–
	0.6 L2.5	brittle	0	–	–
	0.8 L2.5	brittle	0	–	
30 K min^{-1}	0 L2.5	ductile	–	–	
	0.2 L2.5	brittle	24.9	6–16/8–23/1	100/< 1/< 0.5
	0.4 L2.5	brittle	13.9	< 4/< 4/0.5	
	0.6 L2.5	brittle	0	–	–
	0.8 L2.5	brittle	0	–	–
L2.5/BE1.5					
2 K min^{-1}	0 L2.5	ductile		–	
	0.2 L2.5	ductile	–		
	0.4 L2.5	brittle	55.7	8–36/6–18/2	20–40/0.5–3/< 05
	0.6 L2.5	brittle	26.8	< 4/< 4/0.5	< 20/< 0.5/< 0.5
	0.8 L2.5	brittle	0	–	–
30 K min^{-1}	0 L2.5	ductile	–	–	–
	0.2 L2.5	ductile	–		–
	0.4 L2.5	brittle	78.2	10–20/8–36/1–2	20–40/< 1/< 0.5
	0.6 L2.5	brittle	26.2	3–14/0.5–30/0.5	20–40/< 3/< 0.5
	0.8 L2.5	brittle	0	–	–

[a] Fracture types b and d refer to brittle and ductile fracture, respectively
[b] Relative size of the slow-crack-growth zone
[c] Size of fibrils in the slow-crack-growth zone
[d] Size of fibrils in the rapid-crack-growth zone

estimated error of 6%. The $2\bar{L}_c + \bar{L}_a$ data of L95 were calculated from ref. 19.

The periodicity (long period) in the crystal lamellae stacks is obtained from the s value associated with the maximum in the scattered intensity ($I \cdot s^2$) according to the Bragg law. Most of the samples displayed a pronounced single maximum in the $I = f(s)$ curve (*Figure 4*). However, samples with a high content of BE1.5 displayed broad and vague maxima and the calculated long period is associated with a considerable uncertainty, of the order of 10%. *Figure 5* shows long period data for the different blends.

The scattered intensity distributions (*Figure 4*) showed only a single maximum and no indications of bimodality in the long period distribution were found in any of the samples studied. For the binary linear PE blends (L2.5/L144), the long period decreased approximately linearly with increasing content of L2.5, levelling-off at a value of 15.8 nm for pure L2.5 (*Figure 5*). This trend is compatible with a model of separated lamellar crystals, each consisting of separately crystallized high- and low-molar-mass species within the same stack. Another view, also compatible with the SAXS data, is that the low-molar-mass material is incorporated into the crystals which are also composed of high-molar-mass species. However, d.s.c. shows the presence of separate L2.5 crystals of a well-defined and constant melting point in the blends and true cocrystallization is not expected in the binary linear PE blends.

The L2.5/BE1.5 blends showed a more diffuse diffraction pattern for the pure branched polymer (BE1.5). This is due to curvature of crystals and to dispersion of the periodicity, the latter also being confirmed by transmission electron microscopy (TEM)[6]. TEM[6] also showed that L2.5 and BE1.5 cocrystallized in all blends except for the blend of 80% of L2.5, in which partial segregation of L2.5 occurred. The SAXS long period remained essentially constant up to a L2.5 concentration of 50%. Samples with higher L2.5 contents show a narrowing in the small angle diffraction peak and a decreasing trend in long period with increasing L2.5 content.

The tie-chain concentration of the L2.5/BE1.5 blends was calculated assuming that only BE1.5 yielded tie-chains. Equation (6) was used to calculate P_{tc} of BE1.5 (denoted $P_{tcBE1.5}$), and this value was inserted in the following equation to obtain the overall tie-chain concentration (P_{tc}):

$$P_{tc} = \frac{P_{tcBE1.5}(1 - w_{L2.5})w_{cBE1.5}}{(1 - w_{L2.5})w_{cBE1.5} + w_{L2.5}w_{cL2.5}} \quad (7)$$

where $w_{L2.5}$ is the content of L2.5 in the blend, $w_{cDE1.5}$ is the mass crystallinity of BE1.5 and $w_{cL2.5}$ is the mass crystallinity of L2.5. *Figures 6* and *7* show true stress and fracture energy data as a function of the estimated average value of P_{tc}. Both fracture stress and fracture energy increased strongly with increasing tie-chain concentration.

It is known from earlier work that linear PE blends crystallize separately provided that the molar masses are sufficiently different[2]. The blends of L2.5/L95 and

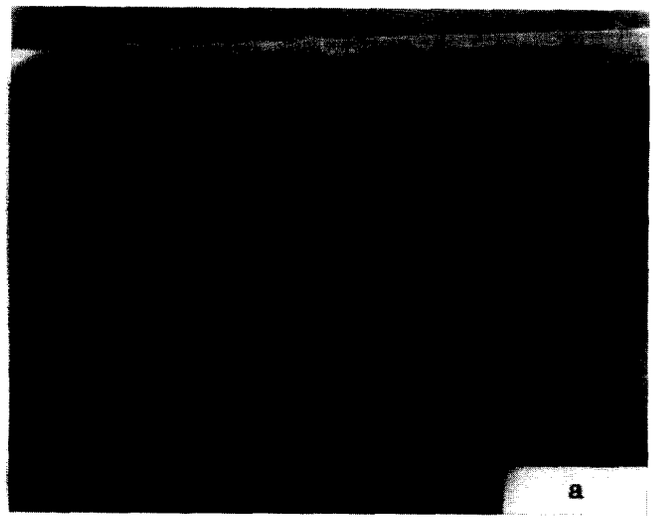

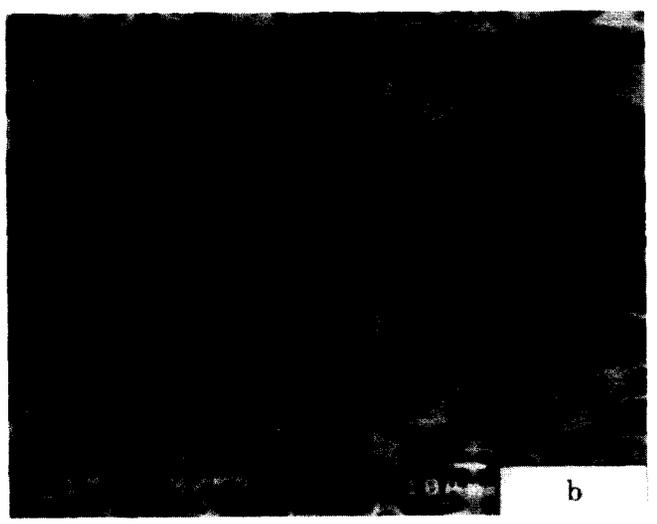

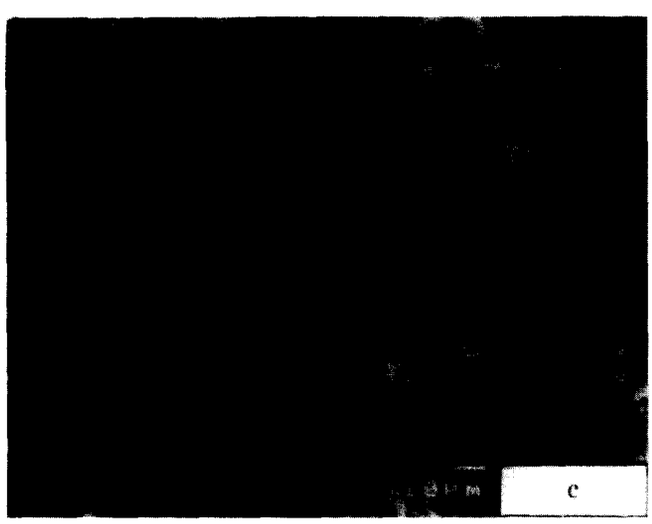

Figure 2 (a) Fracture surface of L2.5/BE1.5 (0.4/0.6) crystallized during a cooling rate of 30 K min^{-1}. The SCG zone is situated adjacent to the notch which is located along the lower edge of the fracture surface. The RCG zone is located at the upper left part of the fracture surface. (b) Fibrils of the SCG zone of L2.5/BE1.5 (0.4/0.6) crystallized during a cooling rate of 30 K min^{-1}. (c) Thin and long fibrils of the RCG zone of L2.5/BE1.5 (0.4/0.6) crystallized during a cooling rate of 30 K min^{-1}. The width and thickness of the fibrils were calculated as the longest and shortest distances over the fibril cross section at its base

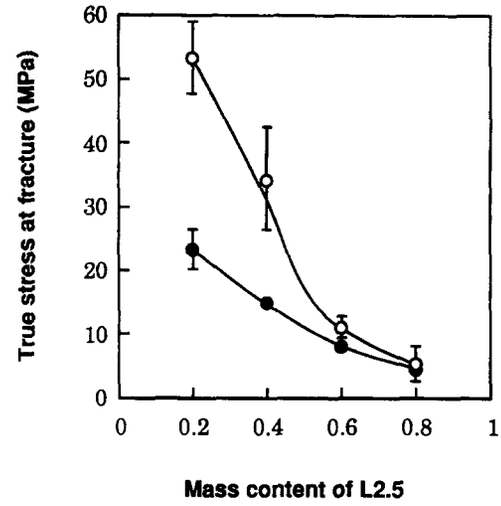

Figure 3 True stress at fracture (average values) as a function of L2.5 content for blends of L2.5/L144 (●) and L2.5/BE1.5 (○) crystallized during cooling at a rate of 2 K min^{-1}. The bars indicate the standard deviation

Table 3 Morphological characterization

Sample	w_c [a]	L (nm)[b]	L (nm)[c]
L2.5 (30 K min^{-1})	0.96	15.8	13.3
L2.5/L144 (2 K min^{-1})			
0/1	0.82	–	35.3
0.4/0.6	0.88	–	21.7 (13.1)[d]
0.8/0.2	0.94	–	14.0 (18.5)[d]
L2.5/L144 (30 K min^{-1})			
0/1	0.76	26.3	34.3
0.2/0.8	0.81	22.8	28.2
0.4/0.6	0.87	20.4	23.7
0.6/0.4	0.90	18.5	21.5
0.8/0.2	0.93	15.7	19.8
L2.5/BE1.5 (30 K min^{-1})			
0/1	0.47	18.5	29.3
0.2/0.8	0.575	21.3	23.4
0.4/0.6	0.68	21.1	21.1
0.6/0.4	0.79	19.7	19.2
0.8/0.2	0.89	18.2	17.2

[a] Mass crystallinity from d.s.c.
[b] Long period ($L_c + L_a$) from SAXS
[c] Long period ($L_c + L_a$) from d.s.c.
[d] Bimodal distribution

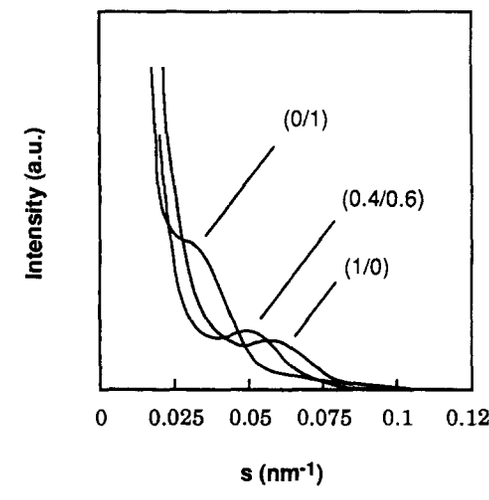

Figure 4 SAXS scattered intensity distribution for a series of L2.5/L144 samples crystallized during a cooling rate of 30 K min^{-1}

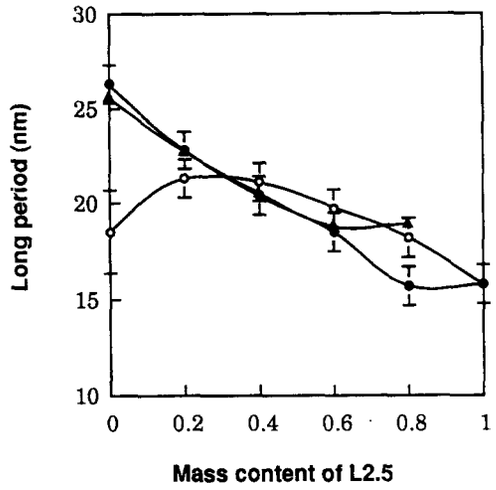

Figure 5 SAXS long period as a function of L2.5 content in blends of L2.5/L144 (●) and L2.5/BE1.5 (○). Bars indicate the accuracy range for deriving the long period from SAXS patterns. L2.5/BE1.5 long periods (▲) were also calculated from TEM data of ref. 6

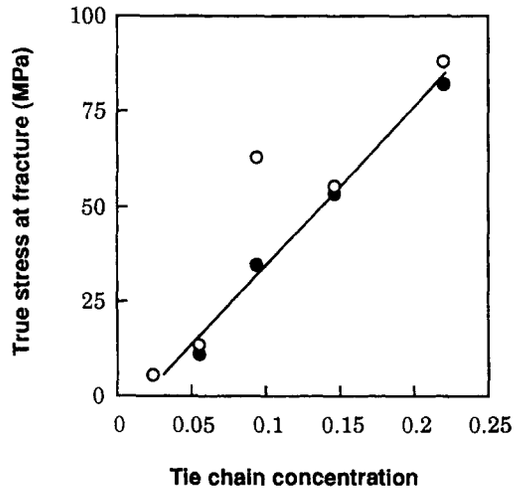

Figure 6 True stress at fracture as a function of the average tie-chain concentration calculated according to equations (6) and (7) for blends of L2.5/BE1.5 cooled at 2 K min^{-1} (●) and 30 K min^{-1} (○)

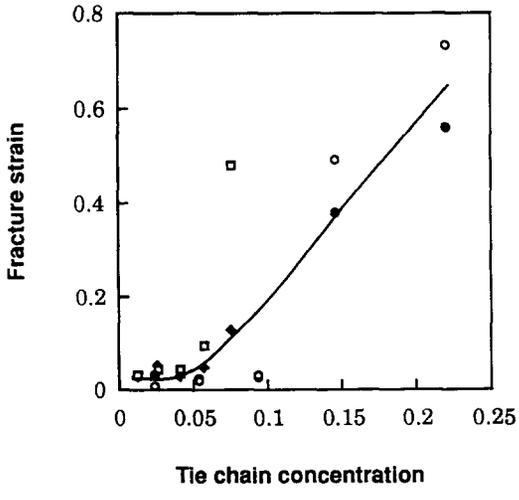

Figure 7 Fracture strain as a function of the average tie-chain concentration calculated according to equations (6) and (7) for blends of L2.5/BE1.5 cooled at 2 K min^{-1} (●) and 30 K min^{-1} (○), and for blends of L2.5/L144 cooled at 2 K min^{-1} (■) and 30 K min^{-1} (□)

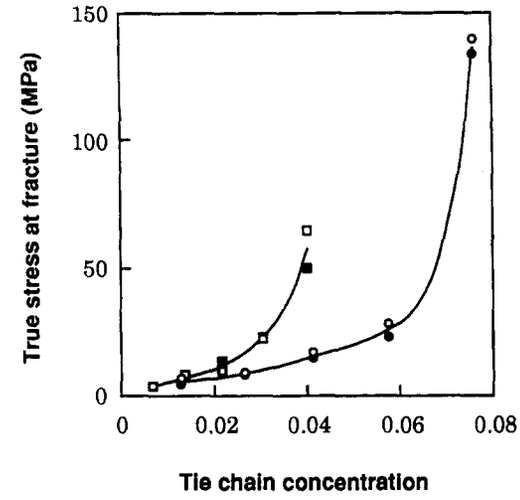

Figure 8 True stress at fracture as a function of the average tie-chain concentration calculated according to equations (6) and (7) for blends of L2.5/L144 cooled at 2 K min^{-1} (●) and 30 K min^{-1} (○), and for blends of L2.5/L95 cooled at 2 K min^{-1} (■) and 30 K min^{-1} (□)

L2.5/L144 consist of separate domains of high molar mass polymer (L144 or L95) and L2.5. *Figure 8* shows that there is no unique relationship between true fracture stress and average tie-chain concentration. The average tie-chain concentrations for the linear blends were calculated according to equation (7), assuming also that only the high molar mass constituent yielded tie-chains. The upturn for L2.5/L95 appeared at distinctly lower average tie-chain concentration values than for L2.5/L144, i.e. a more homogeneous distribution of tie-chains increased the strength. It is therefore suggested that the two different curves for the two series of linear PE blends are due to molar mass segregation.

A comparison between L2.5/BE1.5 and L2.5/L144 (*Figure 7*) indicates only relatively small differences in fracture strain *versus* tie-chain concentration for the two series of polymers. It seems that the major reason why the L2.5/BE1.5 blends are stronger than the L2.5/L144 blends is the higher average tie-chain concentration in the former.

CONCLUSION

The higher fracture resistance of the L2.5/BE1.5 blends compared to the L2.5/L144 and L2.5/L95 blends may be explained by the overall higher tie-chain concentration in the former blends. The lack of a unique relationship between true stress at fracture and average tie-chain concentration for the two linear–linear PE blends also suggests that the distribution of tie-chains in the polymer is important. The fracture resistance, i.e. the true stress at fracture, fracture strain and fracture energy, increased monotonically with increasing content of L2.5 content for all blends.

ACKNOWLEDGEMENTS

This work has been sponsored by the Swedish Board for Technical and Industrial Development (NUTEK), Grants 89-02294P and C656109-2, and the CICYT (Spain), Grant MAT94-0825. The authors thank Neste Polyeten AB, Sweden, for providing the PE grades used in this study and Dr S. Holding, RAPRA Technology Ltd, UK, for the s.e.c. analyses.

REFERENCES

1 Rego Lopez, J. M. and Gedde, U. W. *Polymer* 1988, **29,** 1037
2 Rego Lopez, J. M., Conde Braña, M. T., Terselius, B. and Gedde, U. W. *Polymer* 1988, **29,** 1045
3 Rego Lopez, J. M. and Gedde, U. W. *Polymer* 1989, **30,** 22
4 Conde Braña, M. T., Iragorri Sainz, J. I., Terselius, B. and Gedde, U. W. *Polymer* 1989, **30,** 410
5 Iragorri Sainz, J. I., Rego Lopez, J. M., Katime, I., Conde Braña, M. T. and Gedde, U. W. *Polymer* 1992, **33,** 461
6 Conde Braña, M. T. and Gedde, U. W. *Polymer* 1992, **33,** 3123
7 Gedde, U. W. and Jansson, J.-F. *Polymer* 1985, **26,** 1469
8 Klug, H. P. and Alexander, L. E. 'X-ray Diffraction Procedures for Polycrystalline and Amorphous Materials', Wiley, New York, 1973
9 Christ, B. and Morosoff, N. *J. Polym. Sci., Polym. Phys. Edn* 1973, **11,** 1023
10 Gray, A. P. *Thermochim. Acta* 1970, **1,** 563
11 Hoffman, J. D. *Polymer* 1982, **23,** 656
12 Wunderlich, B. and Baur, H. *Adv. Polym. Sci.* 1970, **7,** 151
13 Tränkner, T., Hedenqvist, M. and Gedde, U. W. *Polym. Eng. Sci.* 1994, **34,** 1581
14 Wunderlich, B., 'Macromolecular Physics: Crystal Structure, Morphology and Defects', Vol. 1, Academic Press, New York, 1973
15 Lustiger, A. and Markham, R. L. *Polymer* 1983, **24,** 1647
16 Huang, Y.-L. and Brown, N. *J. Polym. Sci., Polym. Phys. Edn* 1991, **29,** 129
17 Wignall, G. D., Mandelkern, L., Edwards, C. and Glotin, M. *J. Polym. Sci., Polym. Phys. Edn* 1982, **20,** 245
18 Flory, P. J. 'Statistical Mechanics of Chain Molecules' (reprinted edn), Hanser Verlag, New York, 1988
19 Hedenqvist, M., Angelstok, A., Edsberg, L., Larsson, T. and Gedde, U. W. *Polymer* 1996, **37,** 2887